# MEASURING THE SEISMIC RESPONSE OF AN HTGR CORE MODEL*

J. E. RAKOWSKI, B. E. OLSEN

*General Atomic Company,*
*P.O. Box 81608, San Diego, California 92138, U.S.A.*

## SUMMARY

The seismic program for the design verification of the HTGR core and core support structures was previously introduced in two papers, (1) and (2). These papers described the General Atomic Company HTGR core seismic design approach, covering both analytical methods and results, and the results of seismic tests on core models of various size. The main objectives of this paper are to present (1) the new 1/5 scale full array core model instrumentation including design requirements, calibration and data reduction methods, (2) sample test results obtained with the new instrumentation, and (3) a comprehensive error analysis of the data.

The requirements to obtain core element forces and displacements demanded new and more sophisticated instruments along with new methods for reducing the data. Special applications of eddy current probes determined fuel element rocking angles and vertical separations for investigating the possibility of core disarray during a seismic event, while methods were developed to convert core boundary displacements into core centerline deflections as a means to evaluate the overall core damping.

The advantages of crystal load cells to measure fuel element collision forces and dowel pin forces are discussed and compared to previous methods utilizing calibrated strain gages. Instrument calibration problems are also covered including the need for dynamic as well as static calibration, and the statistical treatment of calibration data.

New test results are presented based on their significance to seismic qualification of the core. Core damping values of up to 40 percent were obtained from free and forced core vibration data utilizing new data reduction methods. The core phase angle response is presented which confirms the core nonlinear resonance behavior found in earlier tests. Fuel element rocking angles are presented for artificial earthquake inputs satisfying the USNRC Regulatory Guide 1.60. The core distribution of dowel pin forces and fuel element collision forces are also given including the load sharing characteristics of the dowels and the distribution of fuel element flat, adge and corner forces for a given earthquake input.

The test data error analysis utilizes a flow chart to identify all systematic and random error sources within the test hardware and data acquisition systems. For the core boundary transducers subject to repeated testing, statistical analysis of the random error in the data is summarized which resulted in one standard deviation of less than 10 percent.

For the relocatable incore instruments, an error model is formulated which combines the system gains, having a random error component, in control system fashion to form a function for the measured response, $u$. The standard deviation in $u$ is then calculated in terms of the known random error in the gains.

The conclusions cover guidelines for design of the core instrumentation, including characterization of the HTGR core model response in terms of damping, resonance frequency, and the distribution of incore forces.

Deviations in core model geometry and transducer calibration data were identified as the largest random error sources. Conclusions from the error analysis are directed at minimizing the data error in future seismic test programs.

* This work was funded in part under U.S. ERDA Contract EY-76-C-3-0167, Project Agreement No. 51.

## 1. Introduction

The seismic program for design verification of the HTGR core and core support structures was previously introduced in two papers [1-2]. These papers described a test program and analytical development program executed simultaneously. The main objective was to provide experimental data in order to verify the analytical models used to develop HTGR core design loads.

To date, most of the testing was performed on a one-fifth scale full array core model, Fig. 1, subjected to uniaxial horizontal excitation. The tests initially focused on evaluating the overall core frequency response, core damping, fuel element collision forces and displacements, and in particular, the lateral support response as a function of the excitation frequency and g-level.

Following this series of tests, a second test program was executed on the model with emphasis placed on obtaining fuel element dowel forces and rocking angles, as well as possible element uplift. In addition, new tests were included to re-evaluate fuel element collision forces and overall core damping which were not satisfactorily obtained earlier.

Several test results are included to illustrate application of the new instrumentation. Finally, a comprehensive error analysis of the test system is presented which provides estimates of the various error sources and total error in the data.

## 2. One-Fifth Scale Model and Excitation

The one-fifth scale test model [2], Fig. 1, represents a 3000 MW(t) HTGR core reference design which contains over 8000 graphite elements including hexagonal fuel elements, reflector elements, plenum elements and core support floor blocks. The core was supported laterally by discrete spring packs representing the actual design while the vertical column supports were replaced by roller bearings allowing the proper lateral freedom.

The full array model represented the reactor core in its cold and fully irradiated state containing maximum gaps between core elements. This condition was expected to generate the most severe response based on preliminary analysis.

Two different waveforms were input to the model as shown in Fig. 2. A sinusoidal sweep at constant g-level in the frequency range of 0-15 hertz was input to obtain the nonlinear response characteristics of the core. Time history excitation in the form of synthesized earthquakes at several g-levels was also utilized to obtain core displacements and forces. These earthquakes satisfied the NRC design response spectra requirements, Regulatory Guide 1.60, and included the amplification of the building structure.

## 3. Instrumentation

Measurement of the fuel element collision forces, dowel forces and rocking angles at various elevations and radial locations in the core was accomplished according to the instrumentation plan in Fig. 3. Transducers were assembled into fuel elements at the elevations shown in five columns of a single fuel region in order to minimize transducer wire interference on the block motion. The five-column package was subjected to a fixed set of tests at each of the core radial positions shown.

### 3.1 Instrument Requirements

The requirements for transducer selection and implementation fell into two basic c categories. The first category concerned the ability of the transducer to accurately measure a dynamic response, and hence resulted in selecting strain gages, quartz load cells and displacement sensors based on their sensitivity, range, and frequency response.

Requirements for these parameters were based on previous test results and analysis.

The same requirements were applied to the transducer assemblies emphasizing that these assemblies do not filter or amplify the actual response which was to be measured. For correct measurement of dynamic response, these requirements were generally satisfied by assuring that the fundamental transducer assembly frequency exceeded the fuel block fundamental frequency and the expected loading frequency.

The remaining requirements were imposed to minimize the effect of the transducers on the physical and dynamic characteristics of the elements to which they were mounted. In essence, transducer arrangements were held to a minimum in terms of size and weight and maximized in stiffness.

In most cases, it was necessary to perforate instrumented fuel elements in order to re-establish the correct mass. Since this might have affected the element stiffness (contact time) and coefficient of restitution, separate collision tests with the instrumented blocks were conducted. The results showed variations only within the scatter band obtained for tests with regular elements. Hence, the changes in the element dynamic characteristics were considered insignificant.

3.2 Design Applications

Measurement of fuel element collision forces in the recent one-fifth scale full-array test program was accomplished by two separate applications of quartz load washers as shown in Fig. 4. In each case, the transducers were mounted on the impacting face and preloaded by an aluminum plate over which was bonded a sheet of graphite one-eighth inch thick. The graphite sheet restored element surface properties and edge geometry. The fundamental preload plate bending frequency was estimated above 4000 hertz, sufficient to eliminate amplification of the shortest duration impact loads.

The load cell design replaced an earlier design where block collision forces were deduced from two strain gages mounted on internal block surfaces and calibrated for impacts. This approach was unsuccessful because the strain wave propagation through the block was different for edge and corner impacts, which resulted in erroneous load interpretation.

The five load cell design provided the added capability of differentiating between flat, edge and corner loads inflicted during an earthquake. The technique for determining block impact orientation is illustrated in Section 6.

The baseline design for measuring fuel element dowel forces is illustrated in Fig. 5. Two strain gages were placed on each of three dowels in a fuel element for measurement of two components of dowel shear force. The dowels were recessed into the blocks to permit the design of a dowel having a scaled stiffness with respect to the prototype fuel blocks. The gages were also recessed to minimize the variation of bending strain as a result of variation in the point of application of shear load along the protruding portion of the dowel. Since the protruding portion of the dowel is small, only insignificant variation in strain gage response occurs from a change in point of application of the load.

A load cell alternative to the dowel strain gages was also utilized in the program. The design illustrated in Fig. 6 employed a two-component shear sensitive quartz load washer simultaneously measuring the net x- and y-axis dowel forces. Although loads were measured successfully, this particular design is not planned for future use in one-fifth scale tests due to the relatively large weight of the instrument. However, multiaxial load

cells of much smaller size have recently been made available with greater potential for dowel force or similar load measurement applications.

The instrument design utilized for fuel element rocking angles is illustrated in Fig. 7. These are eddy current probe displacement transducers which were selected over mechanical probes (LVDTs) and capacitive pickups because of their small size, weight, range, as well as accuracy in measuring relative to an inclined surface. Frequency response was not a problem since block rocking was at a relatively low frequency.

Measurement of three vertical displacements at an interface between stacked elements allowed determination of relative rocking angle, orientation of the rocking axis, and vertical block displacements. Rocking orientation became of interest when a swirling motion of the fuel elements in some regions of the core was visually observed in previous one-fifth scale full array tests.

3.3 Instrument Calibration

Each strain gage and eddy current probe was calibrated over a predetermined range prior to testing. Only a static calibration was performed on the eddy current probes, due to the low frequency content of the displacement input. However, not all transducers provided reliable dynamic response data based on static calibrations in spite of low frequency excitation.

Initially, only static calibration was required for the dowel strain gages, since the dowel bending frequency was well above the expected loading frequency, thus eliminating amplification. Later verification of the gages under simulated test conditions was accomplished using dynamic input loads. The test results in Fig. 8 indicate a 25 percent lower gage sensitivity (pounds per volt) for a dynamic load. This discrepancy was attributed to hysteresis behavior in the gage bonding material.

Similar dynamic tests were performed on the dowel load cell in order to verify the manufacturer's calibration constant. Dynamic loading of the dowel load cell was accomplished by impacting the load cell preload plate with a pendulum equipped with a standard load washer for measurement of the dowel load input. The results in Fig. 9 reveal a measured load cell sensitivity 22 percent less than the manufacturer's value, a difference which was attributed to possible nonuniform preloading of the dowel load cell.

Verification tests were also performed on the fuel element collision force instruments to check the manufacturer's calibration constant. Using the same pendulum, flat impacts were first imposed on the instrumented blocks yielding the results in Table 1. A second set of tests simulated a top edge loading by delivering a concentrated impact one-tenth inch below the top edge of the element. Agreement between the pendulum input load and instrument output load was within six percent for all tests, in this case verifying the manufacturer's calibra- constant.

All derived dynamic calibration constants were used in data reduction since the verification tests simulated behavior under actual test conditions.

4. Data Reduction

Reduction of the test data was performed on a Univac 1110 computer. Aside from applying predetermined calibration factors to the digitized data and constructing frequency response and time history output, new data reduction codes were implemented which are summarized in Table 2. An additional data reduction technique complementing program PKLOAD, but not

computerized at this time, solves for the collision force orientation by utilizing the load measurements recorded on the five load cell block of Fig. 4.

5. Test Results

Test results are presented for the purpose of illustrating the various transducer applications. Further results and discussion of core dynamic behavior is given in reference [2].

Figure 10 shows the fuel element dowel force response for a sinusoidal sweep up and sweep down. The plot is characteristic of a nonlinear structure illustrating a sudden jump in response at the resonance frequencies of 4.2 hertz and 4.7 hertz. These resonances correspond to a lumped fuel element mode and a lumped core support floor mode, respectively.

The figure also shows that, for the sweep down, the jump occurs at a lower frequency. This demonstrates the region of instability for a spring hardening system, as predicted in theory. Similar frequency response behavior was illustrated by all incore and core boundary instruments.

Previous estimates of an overall core damping factor based on linear methods was attempted by measurements of core resonance or the core free vibration decay response. The results were not considered reliable since the resonance curve was typically nonlinear and the free vibration response decays to less than measurable amplitudes in about one cycle.

From the sine sweep tests, however, it was noted that highly lumped core motion took place up to and including resonance. This observation led to construction of the phase lag relationship between the core centerline motion and the test rig input, Fig. 11, and illustrated a 90 degree phase lag at resonance. A single degree of freedom spring-mass system with a viscous damper characterizes near identical phase lag behavior as the experimental data, including the 90° phase lag. Consequently, an effective core damping of about 18 percent of critical was determined by best curve fit of the linear model.

The response data discussed below were obtained for input of a synthesized earthquake with 0.25 g equivalent ground acceleration.

Fuel element rocking angles and their orientation with respect to the excitation axis are shown in Figs. 12 and 13. A maximum rocking angle of 1.3 degrees was observed. The small orientation angle accompanying the rocking angle demonstrates near parallel rocking with the orientation axis. Close inspection of the numerical data showed that in nearly all cases, the larger orientation angles occurred while the rocking angle was a minimum.

Dowel forces represented as the instantaneous sum of forces on three dowels of a fuel element are shown in Fig. 14. A maximum shear force of approximately 17 pounds was measured in the direction of the rig input. Dowel forces of up to thirty percent of this value were measured in a direction perpendicular to the input axis, presumably as a result of net loads on the hexagonal block surfaces not lined up with the excitation. Since forces in both directions may occur simultaneously, the total dowel force is obtained as the vector sum of the two.

Fuel element collision forces recorded with the five component load cell block are shown in Fig. 15. These forces represent the simultaneous net sum of all five load cells. The output for each individual load cell was also recorded separately which allowed determination of the orientations of the impact load on the element face. This is demonstrated by illustrating, in Fig. 16, the distribution of force on the load cells resulting from the impact identified by the arrow in Fig. 15. The loading was classified as a top-edge impact.

Using a predetermined logic in the data reduction, each impact in the response was categorized as either a flat, edge or corner impact. The number of these load cycles which occurred during the excitation was retained for input to subsequent fuel element fatigue analyses. The maximum impact load in Fig. 15 was 142 pounds and corresponds to a flat impact.

## 6. Error Analysis of the Data

This section outlines two methods by which errors in the test data can be estimated. Calculated error values are given for the one-fifth scale full-array test.

In general, the test data contains both systematic and random errors. Systematic errors were distinguished mainly by instrument amplifier drift and were evaluated during null periods of the response. These errors were then removed from the recorded data prior to performing the random error analysis. Random errors were contained in the test model, as well as in the mechanical and instrumentation system components.

When data from repeated tests were available, as in the case of the fixed core boundary transducers, statistical analysis of a sample of measurements was made to calculate the total random error. However, data from in-core transducers were not repeated since relocation of these instruments took place after each test. In this case, the error was obtained by identifying and evaluating the contributing error sources which were subsequently combined.

### 6.1 Statistical Treatment of Repeated Data

The fractional standard deviation represents the total random error in a sample of core boundary transducer data which was determined by eq. (1) using the theory in [3],

$$\hat{s} = \frac{s}{\bar{u}} = \frac{\left[\sum_{i=1}^{N} \frac{(u_i - u_m)^2}{N}\right]^{1/2}}{\bar{u}} \qquad (1)$$

where $N$ = number of repeated measurements

$u_i$ = ith measurement

$u_m$ = mean value or mean curve fit of the data

$\bar{u}$ = the overall mean response in a range of measurements

Application of this technique resulted in a one-standard deviation of eight percent for the core boundary support loads.

### 6.2 Component Error Model

The total random error in the incore data was obtained by evaluating the contributing error sources. These are identified in Fig. 17.

Deviations from the nominal rig input motion occur as a result of the rig control system. The function F(f,g) represents the core dynamics yielding the response $u_M$ as a function of the input motion.

The system gain $G_G$ was included to represent the random deviation of the actual core response, $u_T$, relative to the (hypothetical) response $u_M$ occurring for a perfectly nominal core geometry (core gaps, element dimensions, etc.). The magnitude of a random deviation $u_T - u_M$ was estimated from several isolated tests.

The components inside of the dashed line in the figure represent the conversion of the actual core response, $u_T$ (force, displacement, ...), into an amplified transducer output voltage, $v_A$. This process was interpreted using the calibration data illustrated in the figure, and hence the calibration random error is included at this point.

The other elements of the schematic represent the remaining components of the data acquisition system, namely, a summing circuit, $G_S$, admitting additional signals as in the case of summing forces on three dowels, a peak holding circuit, $G_P$, designed to register and hold the maximum response within a fundamental sampling time of five milliseconds, and the analog to digital function, $G_C$.

The origin of systematic errors are also shown in the figure as well as the procedure for compensation of these errors in producing the final digital signal $V_D^C$. A final random variable, $N_R$, was assumed to enter only in the computer and represents sixty cycle noise or other noise sources observed during null portions of the response.

By applying calibration constants M and B during data reduction, $V_D^C$ was converted into engineering units, hence

$$u_R = V_D^C \frac{M}{\overline{G}_C} + B \qquad (2)$$

where $\overline{G}_C$ is the nominal analog to digital gain factor.

The measured response $U_R$ can be expressed in terms of the system gains in Fig. 17 by making use of the following component equations

$$u_T = G_G\, u_M\,(f,g) \qquad (3)$$

$$V_A = \frac{G_V}{M}(u_T - B) + D \qquad (4)$$

$$V_D = G_C\,(V_P + N_S + N_R) \qquad (5)$$

and $$V_D^C = V_D - \overline{G}_S\,\overline{G}_P\,\overline{G}_C\,D - \overline{G}_C\,N_S \qquad (6)$$

Hence

$$u_R = \frac{G_{CPSVG}}{\overline{G}_C}\,u_M\,(f,g) + \frac{G_C}{\overline{G}_C}\,N_R \qquad (7)$$

where $N_R$ is expressed in engineering units and $G_{CPSVG} = G_C\,G_P\,G_S\,G_V\,G_G$

The standard deviation of $u_R$ is now calculated by substitution of eq. (7) into the following error propagation equation, taken from reference [3].

$$S_{u_R} = \left[\sum_{i=1}^{N}\left(\frac{\partial u_R}{\partial X_i}\right)^2 S_{X_i}^2\right]^{1/2}_{\overline{u},\,\overline{x}_1,\,\overline{x}_2,\,\ldots\,\overline{x}_N} \qquad (8)$$

Letting the $X_i$s represent the system gains which contain a nominal value and a random component

$$G = \overline{G}\,(1 + e)\ ,$$

and including the final random variable $N_R$ whose nominal value is zero, the fractional standard deviation in $u_R$ becomes

$$\hat{S}_{u_R} = \left\{\hat{S}^2_{G_C} + \hat{S}^2_{N_R} + \hat{S}^2_{G_P} + \hat{S}^2_{G_S} + \hat{S}^2_{G_V} + \hat{S}^2_{G_G} + \left(\frac{\overline{g}}{\overline{u}_R}\,\overline{\frac{\partial u_M(f,g)}{\partial g}}\right)^2 \hat{S}^2_g + \left(\frac{\overline{f}}{\overline{u}_R}\,\overline{\frac{\partial u_M(f,g)}{\partial f}}\right)^2 \hat{S}^2_f\right\}^{1/2} \qquad (9)$$

where $\hat{S}_{N_R}$ = the one-standard deviation of the random noise to signal ratio

$\overline{u}_R$ = the mean value of the response, estimated by $u_R$ from a single test

$\overline{\frac{\partial u_M(f,g)}{\partial g}}$ = the variation of response with rig input g-level, estimated by the measured variation of $u_R$ with respect to g-level.

$\overline{\frac{\partial u_M(f,g)}{\partial f}}$ = the variation of response with respect to input frequency, estimated by the measured variation in $u_R$ with respect to frequency

Equation (9) shows that the fractional standard deviation of the measured response, $\hat{S}_{u_R}$, is essentially an RSS sum of the fractional standard deviations of the individual random error sources in the test hardware and instrumentation systems. The last two terms in the expression representing the input g-level and frequency, however, contain weighting coefficients to account for the amplification of core response with respect to these parameters, which in turn depends on the core dynamic characteristics, F(f,g).

Typical one-standard component errors of eq. (9) are summarized in Table 3. The results show that the largest contributors to the total error in the test data were instrument calibration and model geometry errors. Implementation of eq. (9) yielded the one-standard deviations of the total random errors for the incore test data. These are given in Table 4.

## 7. Conclusions

Completion of the one-fifth scale full array core seismic test program, including reduction and error analysis of the data, led to the following conclusions which can be used as an aid to more meaningful data measurements in future seismic tests, namely

(1) The transducers and their applications proved successful for the measurement of core element loads and displacements.

(2) Load cell washers were generally preferred over strain gages for load measurement, however, strain gages were more useful where space was at a minimum. Strain gages proved unsatisfactory when used to predict element collision forces from internal strain measurements.

(3) A method was developed for estimating the overall core damping by calculating the phase angle of the core centerline motion with respect to the rig input motion during sinusoidal excitation.

(4) Dynamic calibration tests on all transducers measuring dynamic load are highly desirable.

(5) Seismic testing should provide sets of repeated tests to obtain the natural spread of data, thereby eliminating the need for error propagation calculations where error sources may be unknown or difficult to estimate.

(6) The largest error sources in the test were found to be instrument calibration error and model geometry errors. Hence, efforts to reduce the random data error should focus on these sources.

(7) On a one-standard deviation basis, the maximum error in the force measurements was 11 percent.

## 8. References

[1] A. J. Neylan, Design Development of the HTGR Core and its Support Structure-Seismic Considerations, Second International Conference on Structural Mechanics in Reactor Technology, Berlin, Germany, 14 September 1973, Vol. 6B.

[2] B. E. Olsen, A. J. Neylan and W. Gorholt, Seismic Test on a One-Fifth Scale HTGR Core Model, Nuclear Engineering and Design, March 1976, Vol. 36, No. 3.

[3] L. G. Parratt, Probability and Experimental Errors in Science, John Wiley and Sons, Ind., New York 1961.

Table I

FUEL ELEMENT LOAD CELL DYNAMIC VERIFICATION

(1a) 2-load cell design

| Test No. | Type of Impact | Σ of Two Load Cells (lb) | Pendulum Load (lb) |
|---|---|---|---|
| 1 | Flat | 326 | 335 |
| 2 | Flat | 294 | 318 |
| 3 | Flat | 258 | 302 |
| 4 | Point | 123 | 144 |
| 5 | Point | 137 | 144 |
| 6 | Point | 137 | 144 |

(1b) 5-load cell design

| Test No. | Type of Impact | Σ of Five Load Cells (lb) | Pendulum Load (lb) |
|---|---|---|---|
| 1 | Flat | 150 | 145 |
| 2 | Flat | 153 | 144 |
| 3 | Point | 157 | 151 |
| 4 | Point | 133 | 152 |

Table II

DATA REDUCTION CODES

| Code | Function |
|---|---|
| PHASE | Calculates the approximate core centerline motion based on the cross core gap and core boundary displacements. The phase angle between the model response and rig input motion is calculated for sinusoidal excitation. |
| ANGLES | Calculates fuel element rocking angles, rocking orientation, and element uplift based on three vertical eddy current probe measurements. |
| PKLOAD | A search routine which selects peak values of the response and determines the number of load cycles based on a pre-specified lower load limit, for example, the endurance limit for graphite. |

Table III

COMPONENT ERRORS

| Symbol | Source | Estimate, % |
|---|---|---|
| $\hat{S}G_C$ | analog-to-digital | 0.3 |
| $\hat{S}H_R$ | extraneous noise | 0.5 |
| $\hat{S}G_P$ | peak holder circuit | 1.0 |
| $\hat{S}G_S$ | summing circuit | 0.5 |
| $\hat{S}G_V$ | instrument calibration | 3 - 10 |
| $G_G$ | model geometry | 4 - 6 |
| $\frac{\bar{g}}{U_R}\frac{\partial U_H}{\partial g}\hat{S}_g$ | input g level | 0.8 |
| $\frac{\bar{f}}{U_R}\frac{\partial U_H}{\partial f}\hat{S}_f$ | input frequency | 1.0 |

Table IV

TOTAL RANDOM ERRORS,
ONE-FIFTH SCALE FULL ARRAY TEST DATA

| Response | (1S) Error, % |
|---|---|
| Boundary Load | 6 |
| Dowel Force | 11 |
| Collision Force | 6 |
| Vertical Displacement | 8 |
| Rocking Angle | 14 |

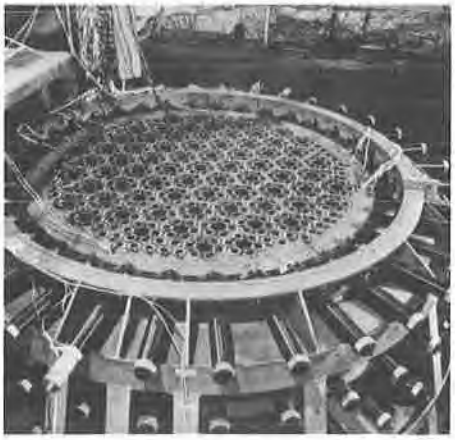

FIGURE 1 One-Fifth Scale Full Array Model and Test Rig

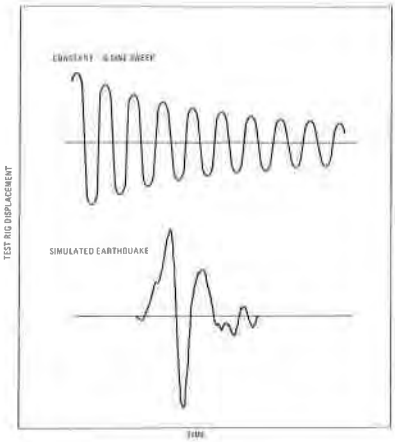


FIGURE 2 Test Rig Excitation

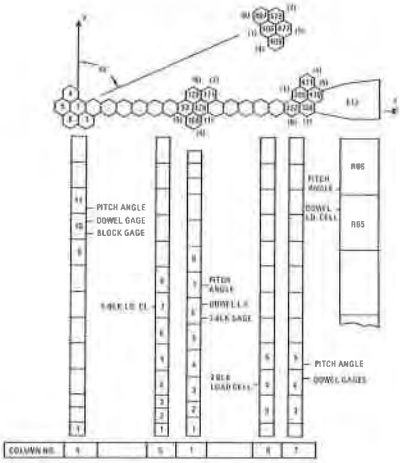


FIGURE 3 Incore Instrument Locations

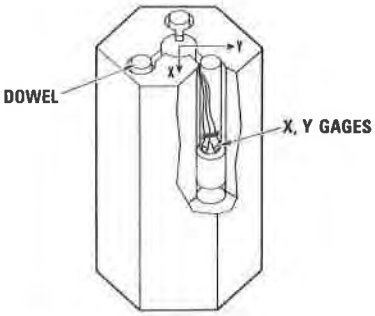


FIGURE 5 Fuel Element Dowel Strain Gage Instrumentation

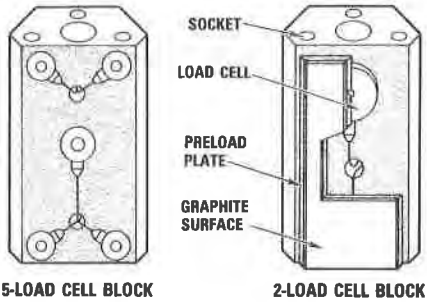


FIGURE 4 Load Cell Instrument for Fuel Element Collision Forces

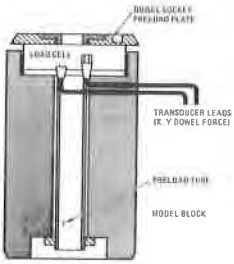


FIGURE 6 Fuel Element Dowel Load Cell

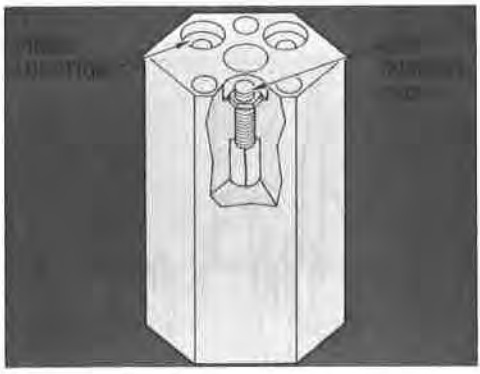

FIGURE 7 Fuel Element Rocking Angle Instrumentation

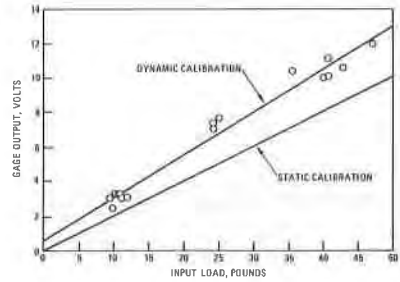


FIGURE 8 Dowel Strain Gage Calibration

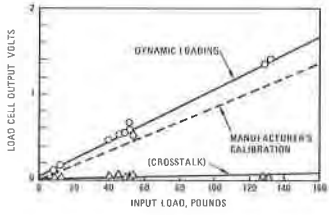


FIGURE 9 Dowel Load Cell Dynamic Verification

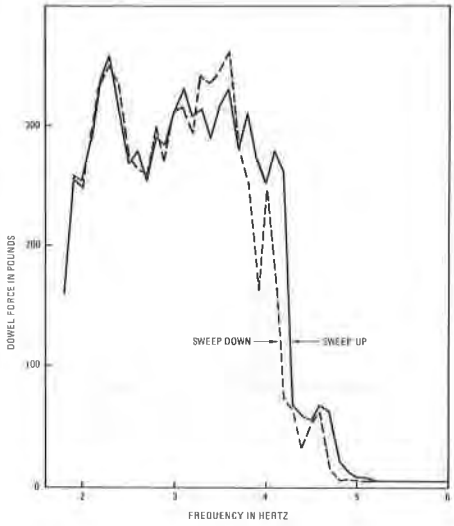


FIGURE 10 Dowel Force Frequency Response

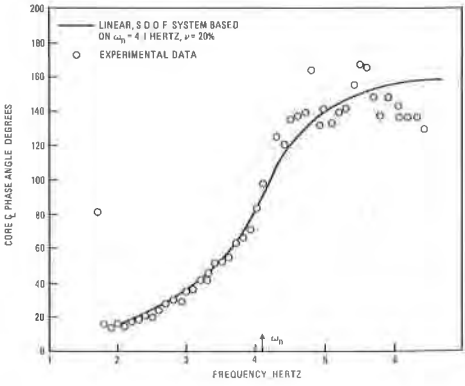


FIGURE 11 Phase Angle Frequency Response of the Core

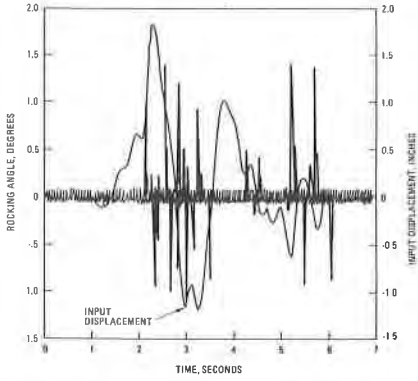


FIGURE 12 Rocking Angle Time History Response

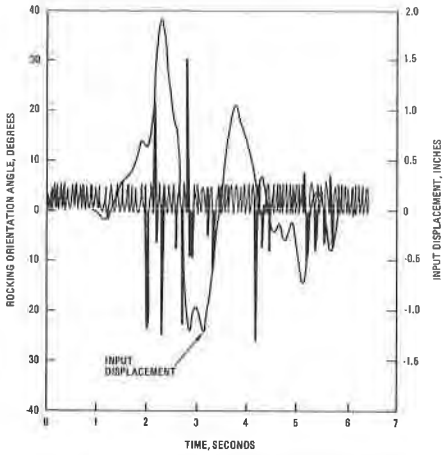


FIGURE 13 Rocking Angle Time History Response

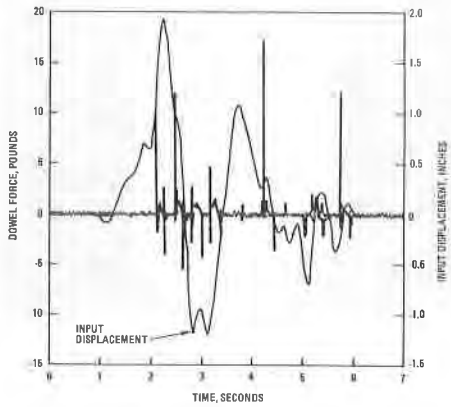


FIGURE 14 Dowel Force Time History Response

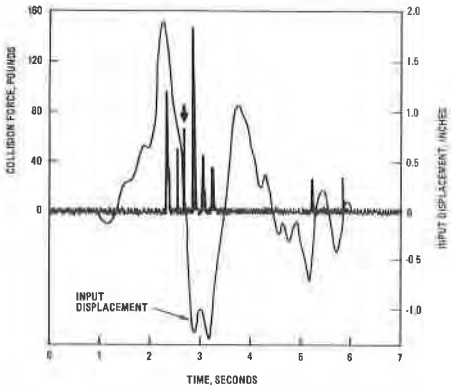


FIGURE 15 Collision Force Time History Response

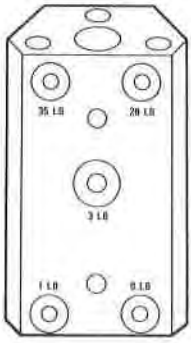


FIGURE 16 Fuel Element Collision Force Orientation

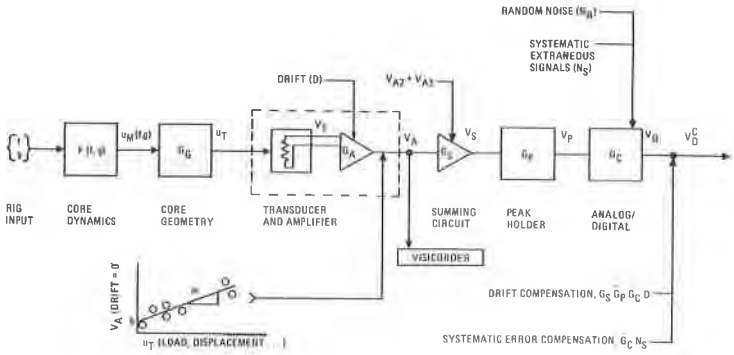


FIGURE 17 Test System Component Error Model